

Electron wavepacket propagation and entanglement in a chain of coupled quantum dots

Georgios M. Nikolopoulos,^{*} David Petrosyan, and P. Lambropoulos[†]

Institute of Electronic Structure & Laser, FORTH, P.O. Box 1527, Heraklion 71110, Crete, Greece

(Dated: October 26, 2018)

We study the coherent dynamics of one- and two-electron transport in a linear array of tunnel-coupled quantum dots. We find that this system exhibits a rich variety of coherent phenomena, ranging from electron wavepacket propagation and interference to two-particle bonding and entanglement. Our studies, apart from their relevance to the exploration of quantum dynamics and transport in periodic structures, are also aimed at possible applications in future quantum computation schemes.

PACS numbers: 03.67.-a, 73.63.Kv, 73.23.Hk

I. INTRODUCTION

Quantum transport is by now an almost generic term encompassing a broad class of phenomena in normally quite distinct areas of physics. Traditionally the term was found in solid state physics [1], while through developments over the last several years, it is commonly found in the context of nonlinear dynamics pertaining to quantum chaos [2], in cold atoms in optical lattices [3, 4], Rydberg atoms strongly driven by microwave fields [5], or even laser-driven multilevel systems [6, 7, 8], the latter dating back twenty five years or so, although the term was never used in that context. Issues of coherent propagation of wavepackets, their interplay with disorder and/or fluctuations, localization, etc. are now discussed in many of these contexts and often interchangeably [9].

A new context, namely low-dimensional nanostructures and in particular quantum dots (QD) [10, 11] has emerged over the last ten or so years which appears to overlap with and in some sense unify several of these areas. Often referred to as artificial atoms [12, 13], they offer the unprecedented possibility to construct at will and explore situations ranging from practically single atom to a fully solid state many-body systems [14, 15, 16, 17, 18, 19, 20, 21, 22, 23, 24]. The nanofabrication possibilities of tailoring structures to desired geometries and specifications, and controlling the number and mobility of electrons confined within a region of space [12, 13, 25, 26], are some of the features that make these structures unique tools for the study of a variety of preselected set of phenomena, not to mention the potential for devices. Given the controllable quantum properties of the electrons in such confined structures, the possibility of their application to schemes of quantum computers [27, 28] has not escaped attention as attested by an ever growing plethora of papers on this general issue [25, 26, 29, 30, 31, 32, 33, 34].

Motivated in part by the connection with quantum computing and in part by the desire to explore the dynamics of wavepackets in periodic structures, we began with the study of such wavepackets in the simplest case of one electron tunneling through an array of QDs. As discussed in some detail below, the problem turns out to have unexpected similarities with an old problem, namely the molecular excitation through a ladder of vibrational levels [6, 7, 8]. Models developed in that context more than twenty five years ago found no application, simply because a vibrational structure is too complex to be amenable to simple models of, for example, equidistant levels or exact levels of a harmonic oscillator. On the other hand, in the present case, one can easily contemplate fabricating almost any desired level and tunneling rates arrangement. Thus, models that were of only academic interest then, now become of practical relevance. At the same time, the equations governing the propagation in a chain of quantum dots are similar to those found in the 1-dimensional (1D) Ising model [35].

Even a slight generalization, namely the presence of one more excess electron in the chain presents an entirely different situation. Its counterpart in multilevel systems does not exist, while it is now the 2D Ising model [35] that is related to the chain of QDs. In our case, however, it is the dynamical rather than the thermodynamic properties of the system that we explore. With two electrons available for tunneling, an additional set of phenomena such as Coulomb blockade, bonding (to be described below), and correlation come into play. Surprisingly, we find that preservation of coherence found in the one-electron case, under a judiciously chosen set of parameters, carries through in the two-electron case. It is this finding that brings in the possible connection with schemes for the quantum computer. Such a possibility could be contemplated when the electron spin is brought into the picture, combined with coherent propagation within a chain of QDs and manipulation of spin-entanglement [29, 30], as discussed in Sec. V.

Even with the high degree of accuracy in nanofabrication technology, issues of randomness and fluctuations [10, 36], originating from more than one physical effect, are an inevitable part of the picture. Their presence, in ad-

^{*}Present address: Institut für Angewandte Physik, Hochschulstrasse 4a, 64289 Darmstadt, Germany

[†]Also at the Department of Physics, University of Crete, Greece

dition to requiring attention with respect to their impact on coherent propagation and entanglement, represents a class of further phenomena related to the well-known localization induced by disorder, and related issues [9]. We have therefore examined some of our basic results in the presence of randomness. Although not necessary for the main arguments of this paper, for the sake of completeness, we have also explicitly included in our analysis the effect of measurement. This has necessitated the adoption of Monte Carlo techniques which are well established in quantum optics and provide a direct account of the effect of a measurement on the system [37, 38, 39].

We would like to state at the outset that, although we do realize that each quantum dot in general has many electrons, it is nevertheless possible to arrange the conditions so that only one electron per dot tunnels, while the rest remain “frozen”. It may not be routine, but on the basis of existing literature [11, 13, 14, 40], it is technologically possible. In fact many papers with proposals for quantum registers employing QDs are based on that very idea [26, 29, 32, 33]. We do also realize that assuming a chain of 10 or 20 dots, as we do in the sections to follow, may indeed stretch present day technological capabilities. We do so, however, in the interest of exploring a number of unusual effects which if not quite feasible today will most likely be feasible tomorrow. But when it comes to entanglement in connection with a quantum register, in the last section of the paper, even two dots fulfill our requirements.

We have structured this paper as follows: In Sec. II we present the mathematical formalism describing 1D chains of QDs, upon which we build the theory of coherent single-electron propagation in Sec. III and two-electron propagation in Sec. IV. In Sec. V we show a scheme for entangling two electrons in the chain via their controlled collision. Our conclusions are summarized in Sec. VI.

II. MATHEMATICAL FORMALISM

The system under consideration consists of a linear array of N nearly identical QDs which are electrostatically defined in a two-dimensional electron gas by means of metallic gates on top of a semiconductor heterostructure, e.g., GaAs/AlGaAs [10, 11, 12]. We describe the evolution of the system using the second-quantized, extended Mott-Hubbard Hamiltonian [17, 20, 22]

$$H = \sum_{j,\alpha} \varepsilon_{j\alpha} a_{j\alpha}^\dagger a_{j\alpha} + \frac{1}{2} \sum_j U n_j (n_j - 1) + \sum_{i<j,\alpha} t_{ij,\alpha} (a_{i\alpha}^\dagger a_{j\alpha} + \text{H.c.}) + \sum_{i<j} V_{ij} n_i n_j, \quad (1)$$

the first two terms being responsible for the intradot effects and the last two terms describing the interdot interactions. Here $a_{j\alpha}^\dagger$ and $a_{j\alpha}$ are the creation and annihilation operators for an electron in state α with the

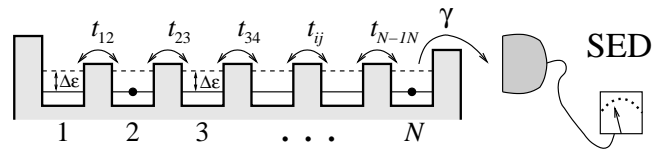


FIG. 1: Schematic drawing of the chain of tunnel-coupled QDs, and the last dot is dissipatively coupled to an external single electron detector (SED).

single-particle energy $\varepsilon_{j\alpha}$ and electronic orbital $\psi_{j\alpha}(\mathbf{r})$, $U = \frac{e^2}{8\pi\epsilon_r\epsilon_0} \int d\mathbf{r}d\mathbf{r}' |\psi_{j\alpha}(\mathbf{r})|^2 |\psi_{j\alpha'}(\mathbf{r}')|^2 / |\mathbf{r} - \mathbf{r}'| \simeq e^2/C_g$, with $C_g \simeq 8\epsilon_r\epsilon_0 R$ being the self-capacitance for 2D disk-shaped QD ($\epsilon_r \simeq 13$ for GaAs), is the on-site Coulomb repulsion, $n_j = \sum_{\alpha} a_{j\alpha}^\dagger a_{j\alpha}$ is the total electron number operator of the j th dot, $t_{ij,\alpha} = \frac{\hbar^2}{2m^*} \int d\mathbf{r} \psi_{i\alpha}^*(\mathbf{r}) \nabla^2 \psi_{j\alpha}(\mathbf{r})$, with m^* being the electron effective mass ($m^* \simeq 0.067m_e$ in GaAs), are the coherent tunnel matrix elements which are given by the overlap of the electronic orbitals of adjacent dots ($j = i + 1$) and thereby can be controlled by the external voltage applied to the gates defining the corresponding tunneling barriers between the dots, and $V_{ij} \simeq U(C/C_g)^{|i-j|}$, with $C \ll C_g$ being the interdot capacitance, describe the interdot electrostatic interaction. Note that in general, the index α refers to both orbital and spin state of an electron. In the Coulomb blockade and tight-binding regime, when the on-site Coulomb repulsion and single-particle level-spacing $\Delta\varepsilon \simeq \frac{\hbar^2\pi}{m^*R^2}$ are much larger than the tunneling rates, $U > \Delta\varepsilon \gg t_{ij,\alpha}$ [41], only the equivalent states of the neighboring dots are tunnel-coupled to each other. Therefore throughout this paper we will consider a single doubly- (spin-) degenerate level per dot ($\alpha \in \{\uparrow, \downarrow\}$), assuming further that the tunneling rates do not depend on the electron spin ($t_{ij,\alpha} = t_{ij}$). In our subsequent discussion, we assume that the matrix elements $V_{ij} = V$ are non-vanishing for nearest neighbors only, $j = i + 1$. Interdot repulsion can be further suppressed in the presence of a nearby conducting backgate, where image charges of excess electrons completely screen the interdot Coulomb repulsion, in which case $V \approx 0$.

We study situations where one or more preselected QDs are initially doped with single electrons (Fig. 1). The preparation of such initial conditions can be accomplished by first applying a large negative voltage to the gates defining the electron confining potentials, while keeping the tunneling barriers low, thereby depleting the chain, and then doping one or more preselected QDs with single electrons by lowering the confining potentials and carefully manipulating the tunneling barriers between the dots and the external electron reservoir [25, 26]. Finally, the system can be isolated by closing the tunnelings between the two ends of the chain and the reservoir. To start the evolution, one then tunes the interdot tunneling rates to the preselected values. This process should, on the one hand, be fast enough on the time scale of t_{ij}^{-1} so that no appreciable change in the initial state of the

system occurs during the switching time τ_{sw} , and, on the other hand, adiabatic so that no nonresonant coupling between the dots is induced: $\varepsilon^{-1}, U^{-1} < \tau_{\text{sw}} < t_{ij}^{-1}$.

To examine the influence of disorder due to structure imperfections, gate voltage fluctuations [11, 13, 14, 42], electron-phonon interactions [36], etc., we allow for random fluctuations of the intradot energy levels and interdot couplings, which would result in a decoherence of the electron wavepacket propagation. Specifically, we model the energy levels ε_j and the interdot couplings t_{ij} as Gaussian random variables, with mean values ε_0, t_0 and variances $\delta\varepsilon, \delta t < t_0$, respectively. To account also for a possible measurement process, we assume the last dot of the chain to be dissipatively coupled to an external single electron detector (SED) with a rate $\gamma_\alpha = \gamma$ (Fig. 1). Such detection can be realized by coupling the last dot to another larger measuring dot at lower potential, which is continuously monitored by a nearby quantum point contact conductor, realizing a broad-bandwidth single electron transistor [11, 43, 44]. Then, the electron tunnels out of the chain into an effective continuum represented by many available, broad (due to the continuous monitoring), empty levels of the measuring dot.

The treatment of this type of problems is amenable to the density operator approach [20, 22]. In the case of only one excess electron present in the system, one has to solve N^2 coupled differential equations (equivalent to the optical Bloch equations) for the density matrix elements. When, however, the initial number n_e of excess electrons in the system is larger than one, $N \gg n_e > 1$, the number of coupled density matrix equations to be solved scales approximately as N^{2n_e} , which is computationally demanding. Having in mind the subsequent application of the method to a chain of QDs doped initially with more than one electron (see below), we adopt here an alternative but equivalent approach based on the Monte Carlo stochastic wavefunctions, which has been well developed and widely employed in the context of quantum optics [37, 38, 39]. Thus, for a set of Gaussian random numbers ε_j, t_{ij} we propagate the wavefunction of the system $|\Psi(\tau)\rangle$ using the effective non-hermitian Hamiltonian $H_{\text{eff}} = H - \frac{i}{2}\gamma n_N$, where H is given by Eq. (1). This involves solving $\sim N^{n_e}$ amplitude equations. The fact that H_{eff} is non-hermitian implies that the norm of the wavefunction is not conserved. The propagation is interrupted by quantum jumps (corresponding to detector clicks in a real experiment) that occur when $\|\Psi(\tau)\|^2 = r$, where r is a uniformly distributed random number, between 0 and 1. Thus, a quantum jump corresponds to the detection of one electron by the detector, while the loss of the electron from the system projects the initial subspace of N QDs sharing n_e electrons, to a subspace of N QDs sharing $n_e - 1$ electrons. The post-jump wave function of the system is thus given by

$$|\Psi\rangle \rightarrow \sum_{\alpha} \frac{a_{N\alpha} |\Psi\rangle}{\sqrt{\langle \Psi | a_{N\alpha}^\dagger a_{N\alpha} | \Psi \rangle}}, \quad (2)$$

where the denominator ensures its renormalization. A

new random number r is then generated which determines the subsequent jump event in our simulations. The propagation is terminated once the system has reached the zero electron state $|0\rangle \equiv |0_1, \dots, 0_N\rangle$. This procedure is repeated and the results are averaged over a large number of independent realizations (trajectories). Thus this method allows one to model both a single experiment outcome, corresponding to a single trajectory, as well as the ensemble average measurement, corresponding to the averaging over many independent trajectories, while the density matrix approach is capable to adequately describe only the latter. Since in the quantum computation schemes, one usually deals with a single measurement on the qubit [27] (with the notable exception of NMR-based QCs), the Monte Carlo approach is more suitable (natural) for modeling the readout from a QC.

III. ONE EXCESS ELECTRON IN THE CHAIN

Let us consider first the simplest case of a chain of QDs initially doped with one excess electron. Since the Hamiltonian (1) preserves the number of electrons and their spin states, the system is restricted throughout its evolution to the one-electron Hilbert space \mathcal{H}_1 , and more precisely to its subspace \mathcal{H}_1^α pertaining to the initial spin state of the excess electron. Thus, the total wavefunction reads

$$|\psi_1(\tau)\rangle = \sum_{j,\alpha} A_j^\alpha(\tau) |j_\alpha\rangle, \quad (3)$$

where $|j_\alpha\rangle \equiv a_{j\alpha}^\dagger |0_1, \dots, 0_N\rangle$ denotes the state where one electron with spin α is located at the j th dot. The time-evolution of $|\psi_1(\tau)\rangle$ is governed by the Schrödinger equation, which yields

$$i \frac{dA_j^\alpha}{d\tau} = \varepsilon_j A_j^\alpha + t_{j-1j} A_{j-1}^\alpha + t_{jj+1} A_{j+1}^\alpha, \quad (4)$$

where $t_{01} = t_{NN+1} = 0$ and $\hbar = 1$. Clearly, the two sets of these amplitude equations, pertaining to the spin up and spin down states, are completely equivalent and decoupled from each other, i.e., the subspaces \mathcal{H}_1^\uparrow and \mathcal{H}_1^\downarrow are closed. As a result, if the excess electron is initially prepared in an arbitrary superposition of spin up and spin down states, $|\psi_1(0)\rangle = A_j^\uparrow |j_\uparrow\rangle + A_j^\downarrow |j_\downarrow\rangle$, the two parts of the wavefunction will evolve symmetrically and independently of each other. This assertion is valid as long as one suppresses all uncontrollable spin-flip processes due to, e.g., presence of stray magnetic fields or spin-phonon coupling, which would otherwise destroy any pure spin state of the electron. Note that if the electrons in the array are to be used as qubits or carriers of quantum information, preserving their spin-coherence over long times becomes vital. This may potentially be realized by applying a strong transverse magnetic field, that would remove the spin degeneracy and make the spin-flip process

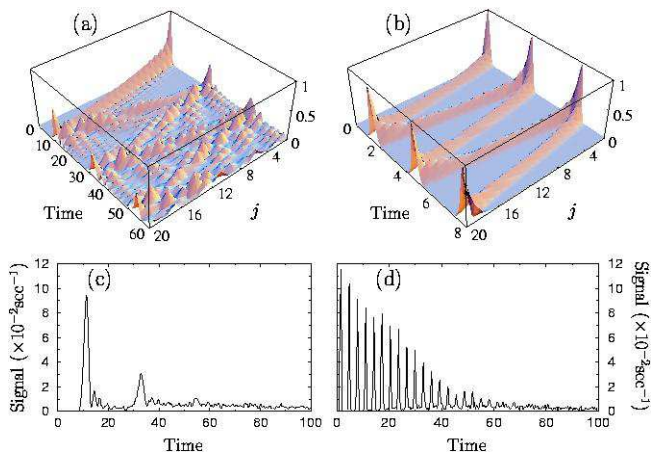


FIG. 2: (a), (b) Single-electron transport in a chain of $N = 20$ QDs with no disorder and dissipation ($\delta\varepsilon = \delta t = \gamma = 0$) for the case of (a) equal couplings, $t_{jj+1} = t_0$, and (b) optimal couplings $t_{jj+1} = t_0\sqrt{(N-j)j}$, between the dots. (c), (d) Monte-Carlo simulations of detector response averaged over 5000 trajectories for the chain with disorder and dissipation ($\delta\varepsilon = 0.1$, $\delta t = 0.05$ and $\gamma = 0.2$) for the case of (a) equal couplings, and (b) optimal couplings between the dots. All parameters are normalized by t_0 and the time is in units of t_0^{-1} .

energetically unfavorable. Experimental measurement of spin-relaxation times indicate sub-MHz rates [42].

In Fig. 2(a) we plot the time-evolution of the occupation probabilities of $N = 20$ QDs along a uniform ($\varepsilon_j = \varepsilon_0, t_{ij} = t_0$), isolated from the environment chain, for the initial state $|\psi_1(0)\rangle = |1_\alpha\rangle$. The initially well localized electron wavepacket seen to propagate along the chain and spread to a larger number of dots, while simultaneously splitting into several smaller components, which is due to the asymmetry of the initial conditions with respect to the electron forward and backward propagation. When the leading edge of the wavepacket is reflected from the end of the chain, its forward and backward propagating components begin to interfere with each other and after several reflections from the boundaries of the chain, this interference causes the complete delocalization of the wavepacket over the entire chain.

The results shown in Figs. 2(a),(b) have been obtained through the numerical solution of Eqs. (4). These solutions, however, can be expressed in an analytical form obtainable through the Laplace transform. If one eliminates the first term via the transformation $A_j^\alpha \rightarrow A_j^\alpha e^{i\varepsilon_j\tau}$, which is equivalent to the interaction picture, taking the Laplace transform of the set of Eqs. (4), leads to

$$isK_j^\alpha(\lambda) - iA_j^\alpha(0) = t_0K_{j-1}^\alpha(\lambda) + t_0K_{j+1}^\alpha(\lambda),$$

where we have assumed equal energies ε_0 and tunneling rates t_0 . Considering the case of only dot 1 occupied initially, which means $A_j^\alpha(0) = \delta_{1j}$, the quantities K_j^α are expressed in terms of the determinants of the coefficients. For N dots, the determinant $\mathcal{D}_N(\lambda)$ is

readily shown to obey the recursion relation $\mathcal{D}_N(\lambda) = \lambda\mathcal{D}_{N-1}(\lambda) + t_0^2\mathcal{D}_{N-2}(\lambda)$ with $\mathcal{D}_0 = 1$ and $\mathcal{D}_1 = \lambda$, which identifies it with the Chebyshev polynomial of the second kind $\mathcal{D}_N(\lambda) = \prod_{k=1}^N(\lambda - \lambda_k)$ known to have the roots $\lambda_k = 2it_0 \cos\left(\frac{k\pi}{N+1}\right)$. The determinants in the numerators of the expressions for $K_j^\alpha(\lambda)$ have similar properties. Taking advantage of this connection with the Chebyshev polynomials, one can, after some algebra, write the solutions for the amplitudes as

$$A_j^\alpha = \frac{2}{N+2} \sum_{k=1}^N \exp\left[-i2t_0\tau \cos\left(\frac{k\pi}{N+1}\right)\right] \times \sin\left(\frac{jk\pi}{N+1}\right) \sin\left(\frac{k\pi}{N+1}\right).$$

It is thus evident that the eigenstates of the coupled system oscillate with incommensurate frequencies corresponding to the roots λ_k of \mathcal{D}_N , which in fact become increasingly densely spaced with increasing N . As a consequence, the system never revives fully to its initial state. This result has also been obtained in an entirely different context of driven multilevel systems [6, 7, 8].

Clearly, it is highly desirable to tailor the parameters of the system so as to achieve a non-dispersive transfer of the single-electron wavepacket between the two ends of the chain. This can be accomplished through the judicious choice of the interdot tunneling matrix elements, namely by choosing t_{jj+1} according to $t_{jj+1} = t_0\sqrt{(N-j)j}$, $j = 1, \dots, N-1$ [Fig. 2(b)], to be referred to hereafter as optimal coupling. Then again, by exploring the properties of the Jacobi polynomials, one can obtain an analytic expression for the amplitudes, which in fact is even simpler, given by the binomial form

$$A_j^\alpha = \binom{N-1}{j-1}^{1/2} [-i \sin(t_0\tau)]^{(j-1)} \cos(t_0\tau)^{(N-j)},$$

while the eigenstates of the system have commensurate frequencies $\lambda_k = t_0(2k - N - 1)$, and the electron wavepacket oscillates in a perfectly periodic way between the first and the last dots, whose occupation probabilities are given, respectively, by $|A_1^\alpha|^2 = \cos(t_0\tau)^{2(N-1)}$ and $|A_N^\alpha|^2 = \sin(t_0\tau)^{2(N-1)}$; a behavior reminiscent of a two-state system, in a generalized sense.

Having established the conditions for the nondispersive transfer of the one-electron wavepacket between the ends of the chain, the next issue is the time-scale of the persistence of the coherence in the presence of disorder and/or fluctuations. In an actual experiment, these effects will also be reflected in the signal detection, i.e., the measurement by a detector connected to one end of the chain. As already mentioned in the previous Section, this process is conveniently modeled through the quantum Monte Carlo technique. Although not necessary for the main issue here, we include it for the sake of completeness, as it represents a mechanism of dissipation inevitably present in an experiment. Continuing thus with

the case of the chain initially doped with one excess electron, $|\psi_1(0)\rangle = |1_\alpha\rangle$, we plot in Figs. 2(c),(d) the results of Monte-Carlo simulations for the detector signal averaged over 5000 trajectories. We chose the amplitudes of the energy-level and tunneling-rate fluctuations to be $\delta\varepsilon = 0.1t_0$ and $\delta t = 0.05t_0$, respectively, which, for typical experimental parameters [41] correspond to $\delta\varepsilon \sim 5 \mu\text{eV}$ and $\delta t \sim 2.5 \mu\text{eV}$. The decay rate γ of the electron from the last dot has been taken to be $\gamma = 0.2t_0 \sim 2.4 \text{ GHz}$. In Fig. 2(c) we show the average detector signal for the case of equal mean couplings between the dots, while in Fig. 2(d) the case of optimal mean couplings is illustrated. Comparing these figures with those corresponding to the isolated uniform chain [Figs. 2(a),(b)], as expected, the detector signal is found peaked around times when the electron occupies the last dot. Over the time scale of $\tau \sim \delta\varepsilon^{-1}, \delta t^{-1}$ the system decoheres significantly due to the inhomogeneity introduced by the energy and coupling fluctuations, while the total occupation probability of the chain decays roughly according to $\sum_j |A_j^\alpha|^2 \simeq \exp(-\gamma\tau/N)$; the latter being the signature of dissipation.

IV. TWO EXCESS ELECTRONS IN THE CHAIN

We consider next a chain of QDs that is initially doped with two excess electrons. In analogy with the one-electron problem, the evolution of the system is restricted to the two-electron sector of the Hilbert space $\mathcal{H}_2^{\alpha\beta}$. We assume that the intradot Coulomb repulsion is so large, $U \gg \varepsilon_j, t_{ij}$, that the two electrons are forced to occupy different dots and thus the states $|j_\alpha, j_\beta\rangle$ corresponding to two electrons at the same dot j are practically forbidden. Then the state-vector of the system at an arbitrary time τ is given by

$$|\psi_2(\tau)\rangle = \sum_{\alpha\beta} \sum_{i < j}^N B_{ij}^{\alpha\beta}(\tau) |i_\alpha, j_\beta\rangle, \quad (5)$$

where $|i_\alpha, j_\alpha\rangle \equiv a_{i\alpha}^\dagger a_{j\alpha}^\dagger |0_1, \dots, 0_N\rangle$ denotes the state where two electrons with spins α and β ($\alpha, \beta \in \{\uparrow, \downarrow\}$) are located at the i th and the j th dots, respectively. The corresponding amplitudes obey the following equations of motion

$$i \frac{dB_{ij}^{\alpha\beta}}{d\tau} = (\varepsilon_i + \varepsilon_j + V_{ij}) B_{ij}^{\alpha\beta} + t_{i-1i} B_{i-1j}^{\alpha\beta} + t_{i+1i} B_{i+1j}^{\alpha\beta} + t_{j-1j} B_{i-1j}^{\alpha\beta} + t_{j+1j} B_{ij+1}^{\alpha\beta}, \quad (6)$$

and obviously, the four subspaces ($\mathcal{H}_2^{\uparrow\uparrow}$, $\mathcal{H}_2^{\uparrow\downarrow}$, $\mathcal{H}_2^{\downarrow\uparrow}$ and $\mathcal{H}_2^{\downarrow\downarrow}$) of $\mathcal{H}_2^{\alpha\beta}$ are governed by equivalent sets of equations. These sets are decoupled from each other, since the Hamiltonian (1) does not contain terms that directly couple different spin states. Note that since the states $|j_\alpha, j_\beta\rangle$ are excluded from state-vector (5), the transient Heisenberg coupling $J_0 = 4t_0^2/U$ between the spins is

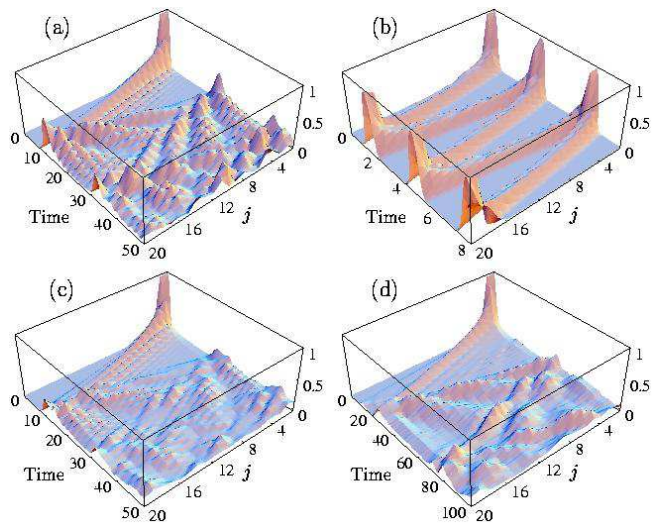


FIG. 3: Two-electron transport in a uniform ($\delta\varepsilon = \delta t = 0$), isolated ($\gamma = 0$) chain of $N = 20$ QDs for the initial state $|\psi_2(0)\rangle = |1_\alpha, 2_\beta\rangle$. (a) Equal couplings between the dots, $t_{jj+1} = t_0$, and (b) optimal couplings $t_{jj+1} = t_0\sqrt{(N-j)j}$ ($j = 1, \dots, N-1$) and no interdot repulsion, $V = 0$. (c) Equal couplings and weak repulsion $V = 0.75$, and (d) equal couplings and strong repulsion $V = 2.5$. Note the different scales of the time axis.

not accounted for in our model. This is justified provided during the time τ over which we consider the system dynamics the probability of this second-order spin-exchange process remains small, $J_0\tau \ll 1$, which in turn requires that $U \gg 4t_0^2\tau$ [45]. Then, due to the linearity of the Schrödinger equation, throughout the evolution each electron will preserve its spin state and the two electrons will not penetrate through one another, remaining thus in principle distinguishable.

Unlike the one-electron case, useful analytic solutions do not seem easy to come by in the presence of a second electron, except for special cases. Also the analogy with the driven multilevel systems exists no longer. Obtained through the numerical solutions of Eqs. (6), in Fig. 3 we plot the time-evolution of the occupation probabilities of the QDs along a uniform, isolated chain for the initial state $|\psi_2(0)\rangle = |1_\alpha, 2_\beta\rangle$. Consider first the case of vanishing interdot Coulomb repulsion $V = 0$. Similarly to the single-electron case, the two-electron wavepacket propagates along the chain, spreads to a larger number of dots and, after several reflections from the boundaries, becomes delocalized over the entire chain, due to the multiple interference of its forward and backward propagating components [Fig.3(a)]. These interference effects can be compensated for by employing the optimal coupling between the dots. Then every time the wavepacket reaches the end of the chain, the two electrons become fully localized at the last two dots [Fig.3(b)]. The system is then formally (mathematically) equivalent to a chain of $2N - 3$ QDs doped with one electron. The solution for

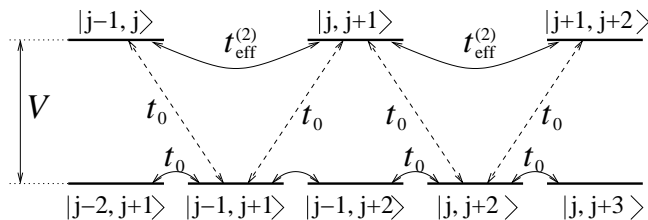


FIG. 4: Energy-level diagram for two-electron states in the chain of QDs.

the amplitudes has the following analytic form

$$B_{ij}^{\alpha\beta} = \left[\frac{(j-i)^2(N-1)(N-2)!}{(i-1)!(j-1)!(N-i)!(N-j)!} \right]^{1/2} [-i \sin(t_0\tau)]^{i+j-3} \cos(t_0\tau)^{2(N-2)-(i+j-3)},$$

while the system has $2N - 3$ distinct, commensurate eigenstates $\lambda_k = t_0(2k - 2N + 2)$, where $1 \leq k \leq 2N - 3$.

Consider now the case of a finite near-neighbor interdot repulsion $V > 0$ and equal tunneling rates between the dots. The magnitude of this repulsion determines the energy mismatch between the states $|i_\alpha, j_\beta\rangle$ corresponding to two electrons occupying adjacent dots, $j - i = 1$, and those corresponding to two electrons separated by one or more empty dots, $j - i > 1$. As we show in Fig. 3(c), for relatively small interdot repulsion $V = 0.75t_0$, the spreading and delocalization of the two-electron wavepacket is accelerated, which is due to inhomogeneity of the eigenenergies of states involved in the system's evolution. For larger interdot repulsion $V = 2.5t_0$, however, we find a rather counter-intuitive behavior of the system: the propagation dynamics of the two-electron wavepacket and its delocalization is slowed down [Fig. 3(d)]. This stems from the fact that when the two electrons are localized at adjacent dots, the corresponding states $|j_\alpha, (j+1)_\beta\rangle$ are coupled directly only to the states $|(j-1)_\alpha, (j+1)_\beta\rangle$ and $|j_\alpha, (j+2)_\beta\rangle$ [Fig. 4]. But if the interdot repulsion is larger than the tunneling rate, $V > t_0$, these transitions are nonresonant and the two electrons appear to be *bonded* with each other. Then, during the system evolution, the latter states are only virtually populated, while the second-order process responsible for the direct transition $|j_\alpha, (j+1)_\beta\rangle \rightarrow |(j+1)_\alpha, (j+2)_\beta\rangle$ is resonant. The effective coupling strength of this transition is given by $t_{\text{eff}}^{(2)} = t_0^2/V < t_0$, and therefore the two-electron wavepacket propagation is slowed down. Since the energy of the two-electron bonded state is larger than that of two separate electrons, the bonded state is not stable and non-adiabatic perturbations, such as collisions with the chain boundaries, gradually destroy it [Fig. 3(d)].

Consider next the time-evolution of the system for the case when the two electrons are initially localized at the opposite ends of the chain, $|\psi_2(0)\rangle = |1_\alpha, N_\beta\rangle$ (Fig. 5). Upon propagation, the electrons collide with each other in the middle of the chain and then sepa-

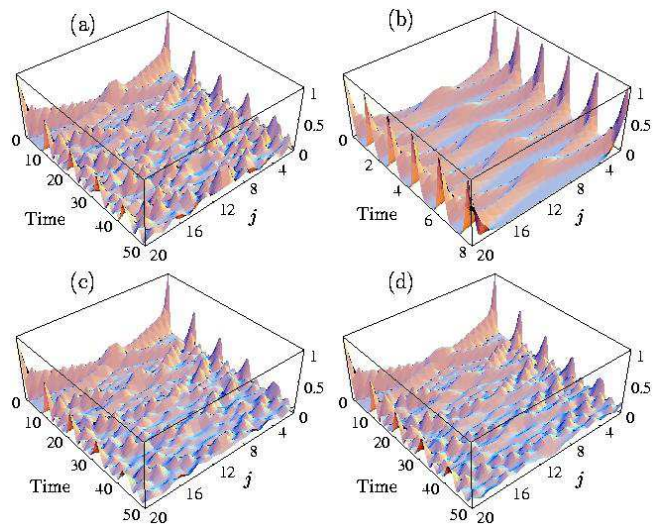


FIG. 5: Two-electron transport in a uniform, isolated chain of $N = 20$ QDs for the initial state $|\psi_2(0)\rangle = |1_\alpha, 20_\beta\rangle$. (a) Equal couplings between the dots, $t_{jj+1} = t_0$, and (b) optimal couplings $t_{jj+1} = t_0\sqrt{(N-j)j}$ ($j = 1, \dots, N-1$) and no interdot repulsion, $V = 0$. (c) Equal couplings and weak repulsion $V = 0.75$, and (d) equal couplings and strong repulsion $V = 2.5$.

rate again. For each electron, the presence of the other represents an effective time-dependent potential barrier, which restricts the number of available dots per electron. Therefore, while after each collision the system partially revives to its initial state, the overall spreading and delocalization of the two wavepackets is slightly enhanced as compared to the case of Fig. 3. Again, choosing the interdot tunneling rates according to the optimal rates $t_{jj+1} = t_0\sqrt{(N-j)j}$, one can compensate for the interference effects and achieve a perfect periodicity in the system dynamics [Fig. 5(b)]. Finally, we note that increasing the interdot Coulomb repulsion strength results in acceleration of delocalization even further and inhibition of occupation of the central dots of the chain where the two electrons collide [Fig. 5(c),(d)].

We proceed now to the application of the quantum jumps method to the two-electron problem. Before the first jump occurs, the evolution of the system is restricted to the two-electron Hilbert space $\mathcal{H}_2^{\alpha\beta}$. Immediately after the jump, the system is projected onto the single-electron Hilbert space \mathcal{H}_1^α where it evolves until the second jump event. The total wavefunction of the system is thus given by $|\Psi\rangle = |\psi_2\rangle + |\psi_1\rangle + |0\rangle$, where $|\psi_{1,2}\rangle$ are defined in Eqs. (3) and (5), respectively. In Fig. 6 we plot the results of our Monte Carlo simulations for the detector signal, averaged over 5000 trajectories. Due to limitations on the computer CPU time, we simulate a chain of $N = 10$ QDs, in which the energy and tunneling-rate fluctuations and the decay rate from the last dot are taken to be the same as in Fig. 2(c),(d), $\delta\varepsilon = 0.1t_0$, $\delta t = 0.05t_0$ and $\gamma = 0.2t_0$. (We do realize that $N = 10 - 20$ may be demanding for present day technology, which, how-

ever, continues evolving.) In the two-electron case, the dynamics of the system is more involved as compared to the single-electron case, and the interpretation of the behavior of the detector signal is more subtle. At small times, while the probability that the first jump has occurred is not yet very large $|\psi_2(\tau)|^2 \lesssim 1$, one can visualize the behavior of the detector signal by comparing the four plots in Fig. 6 with the corresponding 3D graphs in Figs. 3 and 5. One thus sees that the signal is peaked around times when the population of the last dot is maximal. At larger times, however, the averaged over many trajectories signal represents an interplay between the two-electron propagation before the first jump, and single-electron propagation after the jump. Since the jumps occur at random times, the single-electron problem at each trajectory has different initial conditions, and therefore at larger times the detector signal does not have any pronounced structure except for an overall exponential decay with the rate γ/N . Thus in Fig. 6(a) the three pronounced peaks of the signal around $\tau \simeq 7, 18$ and $30 \times t_0^{-1}$ correspond to the arrival of the two-electron wavepacket at the last dot. In Fig. 6(b), where we simulate the case of two-electron bonding via strong interdot Coulomb repulsion $V = 2.5t_0$, the first small peak of the signal around $\tau \simeq 7 \times t_0^{-1}$ corresponds to the small unbonded fraction of the two-electron wavepacket, while the second larger peak represents the delayed arrival of the bonded pair of electrons at the last dot (recall that the effective tunneling rate $t_{\text{eff}}^{(2)}$ for the bonded electron pair is smaller than the single-electron tunneling rate t_0). Our numerical simulations show that increasing the interdot repulsion does indeed strengthen the bonding and reduces the height of the first peak. Next, in Fig. 6(c), where we simulate the case of optimal couplings between the dots, the periodic behavior of the signal at short times reflects the periodic arrival of two-electron wavepacket at the last dot. Finally, in Fig. 6(d), we illustrate the results for the case when the two electrons are initially localized at the opposite ends of the chain. Here, before the first jump has occurred, the second electron is effectively confined in a chain of length $N/2$ QDs. As a result, the signal initially oscillates with twice the frequency as compared to the case of Fig. 6(a), while after the jump, the entire chain becomes accessible to the single remaining electron.

V. ENTANGLEMENT OF TWO-ELECTRONS

Material particles such as electrons represent a promising alternative to circumvent communication and detection loopholes that occur during the tests of Bell inequalities [46]. Despite an ever growing number of theoretical proposals [46, 47, 48, 49], the experimental demonstration of entanglement generation and detection in condensed matter systems is still an open issue. One of the hardest steps towards such a realization is the necessity of controllable spatial separation of the two constituents of an entangled pair [48]. A similar problem would hin-

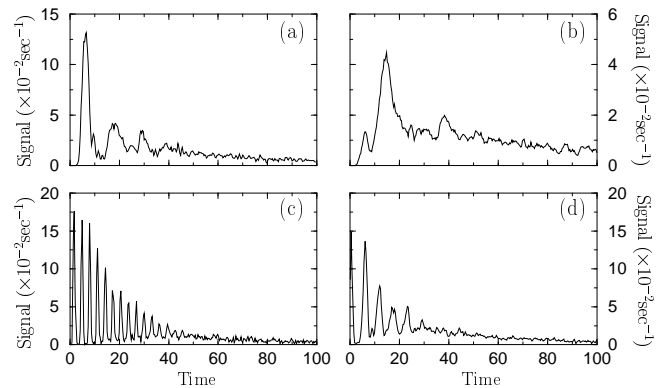


FIG. 6: Monte-Carlo simulations of detector response for the two-electron transport in a chain of $N = 10$ QDs with disorder and dissipation ($\delta\varepsilon = 0.1$, $\delta t = 0.05$ and $\gamma = 0.2$), averaged over 5000 trajectories. In (a), (b) and (c) the initial state is $|\psi_2(0)\rangle = |1_\alpha, 2_\beta\rangle$, and in (d) the initial state is $|\psi_2(0)\rangle = |1_\alpha, 10_\beta\rangle$. Other parameters are: (a), (d) equal mean couplings between the dots and no interdot repulsion, $V = 0$; (b) equal couplings and strong repulsion, $V = 2.5$; (c) optimal couplings and no repulsion, $V = 0$.

der the realization of large-scale solid-state QCs. One of the main difficulties with the existing proposals for integrated QD based QCs [25, 26, 29, 30] is that the qubits (electron spins) interact with the nearest neighbors only, and there is no efficient way of transferring the information between distant qubits (one can SWAP the qubit state with its neighbor qubit, then the latter with the next neighbor, etc., which is inefficient since each SWAP action requires precise dynamical control of the parameters). Our intention in this section is to show that use of the optimal coupling circumvents these difficulties.

We adopt here an entanglement scheme (entangler) proposed in [29, 30], which is based on the exchange interaction in a double-dot system where each QD is occupied by a single electron. When the interdot potential barrier is high, the tunneling is negligible, $t_e \simeq 0$, and the electronic orbitals are well localized at the corresponding dots. By lowering the interdot tunnel barrier, one can induce a finite overlap between the orbitals. Then the two electrons of this “artificial molecule” will be subject to a transient Heisenberg coupling [29, 30, 48]

$$H_s(\tau) = -J(\tau)\vec{S}_L \cdot \vec{S}_R, \quad (7)$$

where $\vec{S}_{L,R}$ are the spin-1/2 operators for the left (L) and right (R) QDs, respectively, and $J(\tau) = 4t_e^2(\tau)/U$ is the effective time-dependent spin exchange constant. If initially the two electrons have opposite spin states, $|\phi\rangle = |L_\uparrow, R_\downarrow\rangle$, and the pulsed Heisenberg coupling is applied for a specific duration such that $\theta \equiv \int J(\tau)d\tau = \pi/2$, the square root of swap action ($\sqrt{\text{SWAP}}$) is realized. Then the resulting state of the system is the maximally entangled state $|\phi\rangle \rightarrow \frac{1}{\sqrt{2}}(|L_\uparrow, R_\downarrow\rangle + i|L_\downarrow, R_\uparrow\rangle)$.

Thus, a possible scheme, capable of producing mesoscopically separated EPR correlated pairs of electrons,

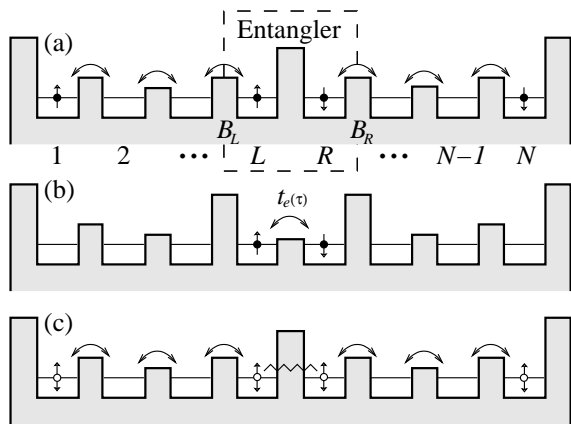


FIG. 7: Three step generation of mesoscopically separated entangled electron pair. (a) In step 1, employing the optimal coupling for the chains $1-L$ and $R-N$, the two electrons are transferred to the entangler. Raising the barriers B_R and B_L , the entangler is temporarily isolated and the two electrons are trapped in dots L and R , respectively. (b) In step 2 a pulsed Heisenberg exchange coupling is applied, by turning on and off the tunneling matrix element $t_e(\tau)$. (c) In step 3 the two electrons are transferred back to dots 1 and N .

relies on the double-dot entangler that is embedded in a long chain of $N = 2M$ coupled QDs. To be specific, let us consider a symmetric structure depicted in Fig. 7(a), in which the entangler, defined by the barriers B_L and B_R , is represented by the two middle dots of the chain, $L = M$ and $R = M + 1$. As discussed at the end of this Section, the exact location of the entangler is not restrictive for the success of the scheme. The entanglement scenario then proceeds in three steps illustrated in Figs. 7(a)-(c), respectively. During the first step [Fig. 7(a)], the potential barrier between the dots L and R is kept high and the exchange coupling is closed, $t_e = 0$. Therefore the two parts of the chain, composed of dots $1-M$ and $(M+1)-N$, respectively, are decoupled from each other. The two unentangled electrons, initially located at dots 1 and N , are coherently transferred to the entangler by employing the optimal coupling in both parts of the chain. At time $\tau = \pi/(2t_0)$, when each electron reaches the corresponding dot of the entangler, the barriers B_L and B_R are pulsed to higher potentials so as to trap the corresponding electron. Note that, since $t_e = 0$, the trapping process need not occur simultaneously for both electrons. At the second step [Fig. 7(b)], the exchange interaction is applied, by adiabatically turning on and off the tunneling matrix element t_e according to $t_e(\tau) = t_e^{\max} \text{sech}[(\tau - \tau^{\max})/\Delta\tau]$, where t_e^{\max} is the peak amplitude of the pulse and $\Delta\tau$ is its width. These parameters must be chosen such that the pulse area θ satisfies $\theta = \pi/2$, which yields $(t_e^{\max})^2 \Delta\tau = \pi U/16$. At the same time, according to the adiabaticity criteria [29], the conditions $\Delta\tau^{-1}, t_e^{\max} \ll \Delta\varepsilon, U$ should be satisfied. Finally, at the third step [Fig. 7(c)], the barriers B_L and B_R are reset to their initial values and the two electrons propa-

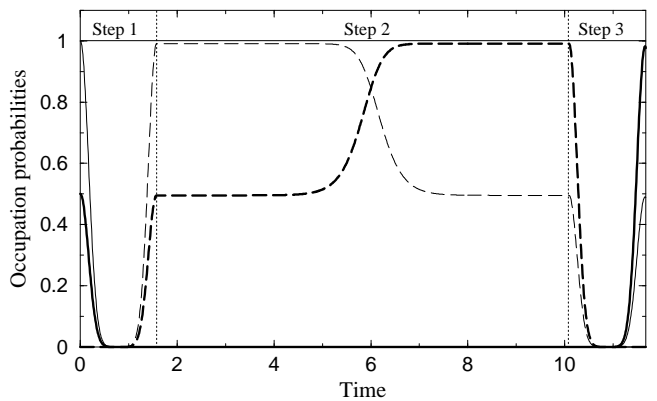


FIG. 8: Monte Carlo simulation of entangled state generation in a chain of $N = 20$ QDs. The initial state is $|\psi_2(0)\rangle = |1_\uparrow, N_\downarrow\rangle$. The occupation probabilities of the two-electron states $|1_\uparrow, N_\downarrow\rangle$ (thin solid line), $|L_\uparrow, R_\downarrow\rangle$ (thin dashed line), $\frac{1}{\sqrt{2}}(|L_\uparrow, R_\downarrow\rangle + i|L_\downarrow, R_\uparrow\rangle)$ (thick dashed line), and $\frac{1}{\sqrt{2}}(|1_\uparrow, N_\downarrow\rangle + i|1_\downarrow, N_\uparrow\rangle)$ (thick solid line) are plotted as functions of time for the three-step process illustrated in Figs. 7(a)-(c), respectively. The parameters are $t_e^{\max} = 6t_0$, $U = 100t_0$ ($\Delta\tau \simeq 0.55t_0^{-1}$) and the optimal coupling is employed separately for each subchain $1-L$ and $R-N$. Other parameters are the same as in Fig. 6.

gate along the chain and after time $\tau = \pi/(2t_0)$ become fully localized at the opposite ends of the chain, at dots 1 and N .

If the two electrons are prepared initially in the opposite spin states, $|\psi_2\rangle = |1_\uparrow, N_\downarrow\rangle$, during the three-step process the system will evolve into the maximally entangled state $|\psi_2\rangle \rightarrow \frac{1}{\sqrt{2}}(|1_\uparrow, N_\downarrow\rangle + i|1_\downarrow, N_\uparrow\rangle)$. If, on the other hand, the two electrons are prepared initially in the same spin state, $|1_\uparrow, N_\uparrow\rangle$ or $|1_\downarrow, N_\downarrow\rangle$, this state will remain unchanged (to within the phase factor $e^{i\theta/2}$). Finally we note that if, during the second step, the exchange pulse area θ is equal to π (instead of $\pi/2$), the two electrons will swap their states $|1_\alpha, N_\beta\rangle \rightarrow i|1_\beta, N_\alpha\rangle$.

We have performed Monte Carlo simulations of the above scenario for an even total number of nearly identical QDs and the initial state $|\psi_2\rangle = |1_\uparrow, N_\downarrow\rangle$. The evolution of the occupation probabilities $|\langle\phi_i|\psi_2(\tau)\rangle|^2$ for the two-electron states $|\phi_0\rangle = |1_\uparrow, N_\downarrow\rangle$, $|\phi_1\rangle = |L_\uparrow, R_\downarrow\rangle$, $|\phi_2\rangle = \frac{1}{\sqrt{2}}(|L_\uparrow, R_\downarrow\rangle + i|L_\downarrow, R_\uparrow\rangle)$, and $|\phi_3\rangle = \frac{1}{\sqrt{2}}(|1_\uparrow, N_\downarrow\rangle + i|1_\downarrow, N_\uparrow\rangle)$ during the three stages of the process are plotted in Fig. 8. One can see that the fidelity of the entangled state generation at the end of the process is very high, $|\langle\phi_3|\psi_2(\tau_{\text{end}})\rangle|^2 \simeq 0.98$. Employing spin-sensitive single-electron transistors [43, 44], one could then use this EPR pair to perform a test of Bell inequalities with material particles (electrons). The controlled two-electron coherent dynamics studied above could be also envisioned in an integrated quantum register. Such a register would be composed of a large number of sub-registers, each containing two or more adjacent qubits represented by spins of single electrons in

individual QDs. The sub-registers are embedded in a two-dimensional *array of empty QDs*. In combination with the mechanism of controlling the tunnel-coupling between the dots, this two-dimensional grid would realize a flexible quantum channel, capable of connecting any pair of qubits within the register. Thus, to transfer the information, one connects distant sub-registers by a chain of empty QDs and arranges the optimal tunnel-coupling between the dots to achieve a non-dispersive propagation of the qubit, followed by its controlled entanglement or SWAP with a target qubit. Note that this scheme is analogous to a proposal for an integrated ion trap based QC [50]. There, in order to circumvent the difficulties associated with single large ion trap quantum register, it was proposed to use many small sub-registers, each containing only a few ions, and connect these sub-registers to each other via controlled qubit (ion) transfer to the interaction region (entangler) represented by yet another ion trap. It would seem that contemplating subregisters consisting of few (as few as two) QDs is no less practical.

Before closing this section, let us address the issue of location of the entangler. Since, as was noted above, the two electrons need not arrive to the entangler simultaneously, it is not necessary to position the entangler in the middle of the chain or synchronize the propagation of the two electrons during the first and the last steps. Actually, the entangler can be realized by any pair of dots in the chain, and in particular, even by the first two dots. Then only the second electron, initially located at dot N should be brought into the entangler to interact with the first electron.

VI. CONCLUSIONS

To conclude, we have studied the microscopic dynamics of one or two electron transport in a linear array of

tunnel-coupled quantum dots. We have shown that coherent electron wavepacket propagation in this system reveals a number of novel, surprising effects, such as suppression or enhancement of interference and spreading, two-electron bonding and collision. We should note that the coherent electron wavepacket propagation in arrays of tunnel-coupled QDs bears many analogies with spin-wave propagation in spin chains [51], electromagnetic wave propagation in nonlinear periodic media [52] and matter-wave propagation in optical lattices, where a transition from superfluid to Mott-insulator phase has recently been observed [3, 4]. With an unprecedented control over system parameters, arrays of QDs allow for studies of numerous coherence and correlation effects in many-body physics. As an example, dynamical localization of electrons is expected to be observed in the arrays with large disorder $\delta\varepsilon, \delta t \sim t_0$ [17, 19]. Our studies are also aimed at possible applications in future quantum computation schemes [27, 28], as many solid state quantum computer proposals involve arrays of interacting quantum dots [25, 26, 29, 30, 31, 32, 33, 34]. We stress that if the electrons in the array are to be used as qubits or carriers of quantum information, preserving their spin-coherence over long times becomes vital. Two-dimensional arrays of electrostatically- and tunnel-interacting quantum dots have also been suggested as an efficient tool for analog computation [53]. In addition, there is presently growing interest in implementing a quantum cellular automata chain [54], in which the computation is performed by applying a sequence of unitary transformations to the input state, upon its propagation through the chain towards the output. Such a chain with tunable couplings between its links would correspond to a universal quantum computer, closely resembling the pioneering idea of Feynman [55] to simulate one physical system by another.

-
- [1] E. Akkermans, G. Montambaux, J.-L. Pichard, and J. Zinn-Justin, eds., *Mesoscopic quantum systems* (North-Holland, Amsterdam, 1995).
 - [2] M.-J. Giannoni, A. Varos, and J. Zinn-Justin, eds., *Chaos and quantum physics* (North-Holland, Amsterdam, 1991).
 - [3] D. Jaksch, C. Bruder, J. I. Cirac, C. W. Gardiner, and P. Zoller, *Phys. Rev. Lett.* **81**, 3108 (1998).
 - [4] M. Greiner, O. Mandel, T. Esslinger, T. W. Haensch, and I. Bloch, *Nature* **415**, 39 (2002).
 - [5] A. Krug and A. Buchleitner, *Phys. Rev. Lett.* **86**, 3538 (2001).
 - [6] J. H. Eberly, B. W. Shore, Z. Bialynicka-Birula, and I. Bialynicki-Birula, *Phys. Rev. A* **16**, 2038 (1977).
 - [7] Z. Bialynicka-Birula, I. Bialynicki-Birula, J. H. Eberly, and B. W. Shore, *Phys. Rev. A* **16**, 2048 (1977).
 - [8] R. Cook and B. W. Shore, *Phys. Rev. A* **20**, 539 (1979).
 - [9] B. Kramer and A. MacKinnon, *Rep. Prog. Phys.* **56**, 1469 (1993).
 - [10] L. Jacak, P. Hawrylak, and A. Wijs, *Quantum Dots* (Springer-Verlag, Berlin, 1998).
 - [11] L. Kouwenhoven, C. Marcus, P. McEuen, S. Tarucha, R. Westervelt, and N. Wingreen, in *Mesoscopic Electron Transport*, edited by L. Sohn, L. P. Kouwenhoven, and G. Schön (Kluwer Academic, Dordrecht, 1997), vol. 345 of *Series E: Applied Sciences*, pp. 105–214.
 - [12] L. P. Kouwenhoven, D. G. Austing, and S. Tarucha, *Rep. Prog. Phys.* **64**, 701 (2001).
 - [13] S. M. Reimann and M. Manninen, *Rev. Mod. Phys.* **74**, 1283 (2002).
 - [14] W. G. van der Wiel, S. D. Franceschi, J. M. Elzerman, T. Fujisawa, S. Tarucha, and L. P. Kouwenhoven, *Rev. Mod. Phys.* **75**, 1 (2003).
 - [15] N. C. van der Vaart, S. F. Godijn, Y. V. Nazarov, C. J. P. M. Harmans, J. E. Mooij, L. W. Molenkamp, and C. T. Foxon, *Phys. Rev. Lett.* **74**, 4702 (1995).
 - [16] L. P. Kouwenhoven, F. W. J. Hekking, B. J. van Wees, C. J. P. M. Harmans, C. E. Timmering, and C. T. Foxon,

- Phys. Rev. Lett. **65**, 361 (1990).
- [17] C. A. Stafford and S. Das Sarma, Phys. Rev. Lett. **72**, 3590 (1994).
- [18] R. Kotlyar, C. A. Stafford, and S. Das Sarma, Phys. Rev. B **58**, R1746 (1998).
- [19] C. A. Stafford, R. Kotlyar, and S. Das Sarma, Phys. Rev. B **58**, 7091 (1998).
- [20] S. A. Gurvitz and Y. S. Prager, Phys. Rev. B **53**, 15932 (1996).
- [21] S. A. Gurvitz, Phys. Rev. B **57**, 6602 (1998).
- [22] M. R. Wegewijs and Y. V. Nazarov, Phys. Rev. B **60**, 14318 (1999).
- [23] K. Kang, M.-C. Cha, and S.-R. E. Yang, Phys. Rev. B **56**, R4344 (1997).
- [24] Z. Yu, A. T. Johnson, and T. Heinzl, Phys. Rev. B **58**, 13830 (1998).
- [25] J. M. Elzerman, R. Hanson, J. S. Greidanus, L. H. Willems van Beveren, S. De Franceschi, L. M. K. Vandersypen, S. Tarucha, and L. P. Kouwenhoven, Phys. Rev. B **67**, 161308(R) (2003).
- [26] L. Vandersypen, R. Hanson, L. Willems van Beveren, J. Elzerman, J. Greidanus, S. De Franceschi, and L. Kouwenhoven, in *Quantum Computing and Quantum Bits in Mesoscopic Systems* (Kluwer Academic, Dordrecht, 2002).
- [27] M. A. Nielsen and I. L. Chuang, *Quantum Computation and Quantum Information* (Cambridge University Press, Cambridge, 2000).
- [28] A. Steane, Rep. Prog. Phys. **61**, 117 (1998).
- [29] D. Loss and D. P. DiVincenzo, Phys. Rev. A **57**, 120 (1998).
- [30] G. Burkard, D. Loss, and D. P. DiVincenzo, Phys. Rev. B **59**, 2070 (1999).
- [31] P. Zanardi and F. Rossi, Phys. Rev. Lett. **81**, 4752 (1998).
- [32] X.-Q. Li and Y. Arakawa, Phys. Rev. A **63**, 012302 (2000).
- [33] T. Tanamoto, Phys. Rev. A **61**, 022305 (2000).
- [34] M. Bayer, P. Hawrylak, K. Hinzer, S. Fafard, M. Korzukinski, Z. R. Wasilewski, O. Stern, and A. Forchel, Science **291**, 451 (2001).
- [35] R. R. E. *et al.*, *Principles of nuclear magnetic resonance in one and two dimensions* (Clarendon, Oxford, 1987).
- [36] T. Takagahara, J. Lumin. **70**, 129 (1996).
- [37] J. Dalibard, Y. Castin, and K. Mølmer, Phys. Rev. Lett. **68**, 580 (1992).
- [38] R. Dum, P. Zoller, and H. Ritsch, Phys. Rev. A **45**, 4879 (1992).
- [39] M. B. Plenio and P. L. Knight, Rev. Mod. Phys. **70**, 101 (1998).
- [40] X. Hu and S. Das Sarma, Phys. Rev. A **64**, 042312 (2001).
- [41] Typically, in ~ 50 nm size GaAs/AlGaAs QDs, separated from each other by ~ 100 nm, one has $t_{ij} \sim 0.05$ meV, $\Delta\varepsilon \sim 0.4$ meV, $U \sim 10$ meV, and at dilution-refrigerator temperatures $T \sim 2-10$ mK the thermal energy is $k_B T \sim 0.2 - 1$ μ eV [11].
- [42] T. Fujisawa, Y. Tokura, and Y. Hirayama, Phys. Rev. B **63**, R081304 (2001).
- [43] R. J. Schoelkopf, P. Wahlgren, A. A. Kozhevnikov, P. Delsing, and D. E. Prober, Science **280**, 1238 (1998).
- [44] W. Lu, Z. Ji, L. Pfeiffer, K. W. West, and A. J. Rimberg, Nature **423**, 422 (2003).
- [45] In the opposite limit of large and controllable Heisenberg-type spin-exchange coupling between pairs of electrons at adjacent sites, one can realize a controlled entanglement between two qubits, each represented by a spin state of the corresponding electron [29].
- [46] X. Maitre, W. D. Oliver, and Y. Yamamoto, Physica E **6**, 301 (2000).
- [47] D. S. Saraga and D. Loss, Phys. Rev. Lett. **90**, 166803 (2003).
- [48] X. Hu and S. Das Sarma, *Double quantum dot turnstile as an electron spin entangler*, cond-mat/0307024.
- [49] P. Zhang, Q.-K. Xue, X.-G. Zhao, and X. Xie, *Generation of spatially-separated spin entanglement in a triple quantum dot system*, cond-mat/0307037.
- [50] D. Kielpinski, C. Monroe, and D. J. Wineland, Nature **417**, 709 (2002).
- [51] J. Cavanagh, W. J. Fairbrother, A. G. Palmer, and N. J. Skelton, *Protein NMR Spectroscopy: Principles and Practice* (Academic, San Diego, 1996).
- [52] G. Kurizki, A. Kozhekin, T. Opatrny, and B. Malomed, in *Progress in Optics*, edited by E. Wolf (Elsevier, North-Holland, 2001), vol. XXXXII, pp. 93-146.
- [53] N.-J. Wu, H. Lee, Y. Amemiya, and H. Yasunaga, IEICE Trans. Electron. **E82C**, 1623 (1999).
- [54] C. S. Lent, P. D. Tougaw, and W. Porod, Appl. Phys. Lett. **92**, 714 (1993).
- [55] R. P. Feynman, Int. J. Theor. Phys. **21**, 467 (1982).